Modeling and Simulation of Oil Transport and Transformation for Studying Piston Deposits

by

Thomas Patrick Grimley

B.S., Mechanical Engineering
The University of Texas at Austin (2007)

Submitted to the Department of Mechanical Engineering
in partial fulfillment of the requirements for the degree of

Master of Science in Mechanical Engineering

at the

MASSACHUSETTS INSTITUTE OF TECHNOLOGY

June 2009

Author .....
Department of Mechanical Engineering
May 8, 2009

Certified by .....
Victor W. Wong
Principal Research Scientist
Thesis Supervisor

Accepted by .....
David E. Hardt
Chairman, Department Committee on Graduate Theses

Modeling and Simulation of Oil Transport and Transformation for Studying Piston Deposits

by

Thomas Patrick Grimley

Submitted to the Department of Mechanical Engineering
on May 8, 2009, in partial fulfillment of the
requirements for the degree of
Master of Science in Mechanical Engineering

Abstract

The formation of carbonaceous engine deposits is a long standing and well documented phenomenon limiting the lifetime of diesel engines. Carbon remnants coat the surfaces of the combustion chamber, piston, and valves. As piston deposits thicken, they increase the risk of a power cylinder seizure. More restrictive emission standards require careful power cylinder design to control piston deposits, specifically in the top land and top ring groove.

Experimental studies on heavy duty diesel engines show a non-uniform pattern of carbon deposits on the top land. The degradation of engine lubricant is typically understood to be source of deposits. A theoretical study was begun to understand the effects of harsh operating environment that leads to degradation. A thin-film, transient, mass and heat transfer simulation of the top land was formulated, which utilizes the results of a combustion chamber CFD simulation as input data.

Thesis Supervisor: Victor W. Wong
Title: Principal Research Scientist

Acknowledgments

My time at MIT has been both personally and professionally rewarding due to the support and friendship of many people.

I would like to thank my advisor Dr Victor W. Wong for his guidance and support. Also, I would like to thank my project sponsors Volvo Powertrain, Lubrizol, and Federal Mogul. Project meetings were always something to look forward to.

In addition, I would like to thank Pelle[1] of Pelles C and Bastian Bandlow[2] of MATLAB Central for creating a C99 Windows compiler and describing how to use them in MATLAB, respectively.

I would like to thank my many friends here, especially those in the Mechanical Engineering and Chemistry departments, who always provide a nice retreat from my academic life.

Lastly, I would like to thank my mother and father, whose support I can always count on.

[1] http://www.smorgasbordet.com/pellesc/

[2] http://www.mathworks.com/matlabcentral/fileexchange/20877

THIS PAGE INTENTIONALLY LEFT BLANK

Contents

List of Figures

THIS PAGE INTENTIONALLY LEFT BLANK

List of Tables

THIS PAGE INTENTIONALLY LEFT BLANK

Chapter 1

Introduction

The formation of carbonaceous engine deposits is a well documented phenomenon limiting the lifetime of diesel engines. Carbon remnants coat the surfaces of the combustion chamber, piston, and valves. Deposit formation prevents an engine from running at peak performance and can shorten engine lifetime.

1.1 Motivation

Experimental studies of pistons show an uneven distribution of carbon deposits on the piston surface above the top ring on the top land (shown in Figure 1-1). The exact mechanism for carbon deposits is not yet conclusively known, but their problems are well known. Uncontrolled deposit formation typically results in loss of efficacy of oil control rings and can cause rapidly increase oil consumption rates. Burning lubricating oil results in poorly conditioned emissions. As deposit layers thicken, friction between the piston and liner increases, causing scuffing and eventually violent failure as the power cylinder seizes.

Emissions requirements initiated by the U.S. Environmental Protection Agency (EPA) in the Clean Air Act and subsequent amendments, as well as equivalent agencies world-wide[1], demand careful attention to the various sources of carbon dioxide, ni-

[1]For instance, the European Union's Directive 70/220/EEC first established air pollution stan-

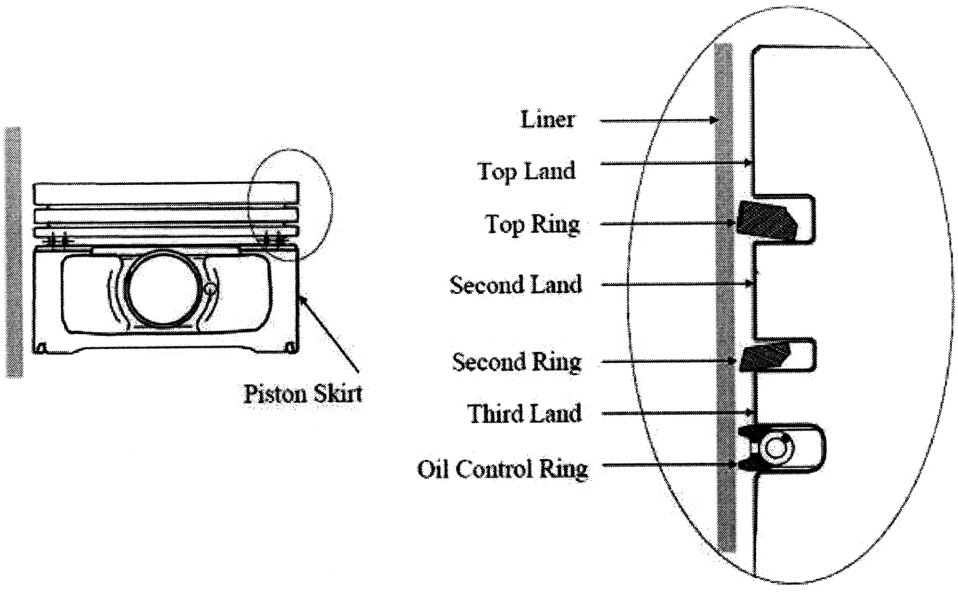

Figure 1-1: Ring-pack schematic adapted from [27]

trous oxides and particulate matter [2, 22, 38]. Understanding the sources of these emissions is a first step in designing a system which produces fewer pollutants and meets current and future standards [28].

A chemical analysis of carbon deposits formed on piston lands during use in diesel engines reveals that they result from the degradation of lubricants [31, 17, 8, 15]. Lubricating oils contain a variety of chemicals to improve their performance, but over hours of intense heat, pressure, and shear forces, these chemicals break down into degradation products. Degradation products are an undesirable outcome because the oil loses its effectiveness and a great deal of work has gone into balancing the additive load and combating the effects of degradation.

Modern lubricants used in diesel engines are a mixture of 5-8% viscosity modifiers, 12-18% additives, and the balance (83%) base oil[2] [34, 9]. Additive packages are comprised of specialized molecules, typically heavy in metallic elements such as zinc,

dards for motor vehicles [1]

[2]Although additives can compromise nearly 20% of "additive" material this does not mean 20% of chemical materials are additives because additive packages generally come as oil solutions of the active ingredients.

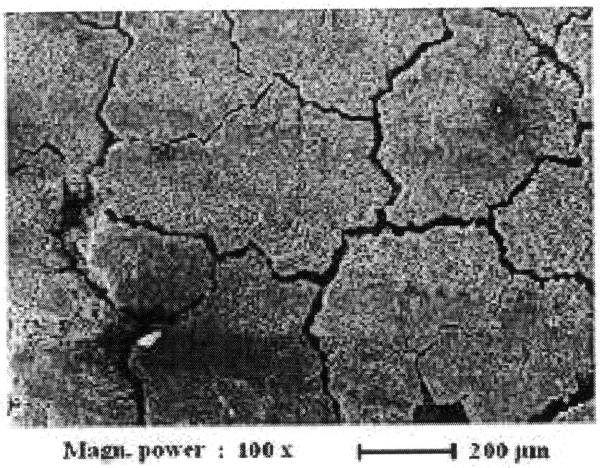

Figure 1-2: Morphology of carbon deposits taken from [17]

calcium, and magnesium, and phosphates and sulfates which contribute to ash content. Because of the problems introduced by these compounds, alternative biodegradable lubrication and fuel formulations utilizing vegetable oils have been proposed [19, 38, 42]. As emissions standards have become stricter, some focus has shifted to the effect of these unburned compounds in after-treatment systems such as diesel particulate filters [50, 24, 33, 21, 7].

The vast majority of published work on carbon deposit formation is experimental, likely due to the extremely complex chemical pathways involving thousands of species and reactions (described to some extent in Chapter 2). Literature ranges from fundamental [14, 23] to applied [31, 30, 11, 10]. Various properties of deposits (such as thermal conductivity [36], morphology [14, 17], and chemical composition [30, 23]) have been studied using methods such as Thermo-Gravimetric Analysis [38, 17], Infrared Spectroscopy [17], Laser Induced Fluorescence [39], and Electron Microscopy [17]. However, it is consistently found that carbon deposit formation depend heavily on fuel type, lubrication oil, and engine environment.

1.2 Objectives

A previous study [34] began this analytical inquiry into the cause of this pattern and found that blow-by gases were the culprit of the *oil distribution* and this work attempts to extend that knowledge by attempting to predict *carbon distribution* through the formation of a full physical model and framework for adding a chemical model. As the previous section emphasized, there is not a clear path for modeling carbon deposit formation. Instead, this work will only attempt to define the environment as a function of space and time.

A statistical study comparing deposit formation under experimental conditions to those "carbon potential" parameters from a simulation of the same conditions should help to validate the model and allow for inexpensive parametric studies of operating conditions.

Succinctly, the main objective of this work:

> *Create a simulation tool (*TLOTTS[3]*) which makes accurate, detailed local predictions of lubricant distribution, vaporization, concentration, and temperature on the top land.*

This simulation requires combustion calculations that include the top land crevice volume flow and temperatures, as in [34, 41]. These are to be carried out either by MIT or by project sponsors. The final simulation needs the following characteristics:

- The final simulation has to be fast enough that it can be deployed on a typical desktop computer and run to convergence (hundreds of engine cycles or hundreds of thousands of time steps)
- Have an open framework such that additional phenomena can be applied (especially chemical)
- Include vaporization mass loss by species

[3]Top Land Oil Transport and Transformation Simulation

- Allow variable oil formulations, piston geometry, and combustion properties

There are many effects not included by this simulation, such as any chemical reactions, degradation by shear, contact of oil film with the liner wall, or the effects of the thermal resistance of deposits. Instead, it deals solely with the detailed Newtonian mechanics and heat transfer calculations as they apply to the top land oil.

1.3 About This Document

This document was prepared using the freely available LaTeX editor LEd (available at `http://www.latexeditor.org/`) and the MiKTeX LaTeX distribution (available at `http://miktex.org/`). It is available online at `http://dspace.mit.edu/`

THIS PAGE INTENTIONALLY LEFT BLANK

Chapter 2

Background

The focus of this work was to extend previous knowledge of oil flow on the top land to approach a full chemical model of carbon formation on the top land. To this end, a full thermal and composition model was integrated, with the intention to set the stage for integration with much more complex chemical calculations. Because the modeling efforts did not include the full chemical phenomenon, this section is merely an overview of potential pathways for chemical transformation and oil transport. In addition, most of the mechanisms described here will equally apply to piston liner transformations, and vice-versa.

2.1 Lubricant Properties

Modern engine lubricants must perform a variety of functions such as friction reduction, wear protection, thermal management, cleaning, anti-foaming, anti-corrosion, sealing, etc. To meet these goals, lubricants typically used in diesel engines are a mixture of base oil and additives. The additive packages in modern oils are highly specialized groups of chemicals each addressing a particular functional requirement of the lubricating oil. Additive companies and lubricating oil producers work closely to balance the effects of each component.

2.1.1 Base Oils

Key physical properties are viscosity (highly temperature dependent) and flash point. Oxidation stability is a primary concern. Base oils are typically processed to improve their consistency through processes such as hydrocracking, dewaxing, solvent extraction, or similar [9, 29].

2.1.2 Additives

Aside from viscosity modifiers and pour-point depressants[1], additives primarily deal with the chemical aspects of lubricating oils. In general, they improve oxidation, corrosion, or deposit formation resistance. Common types and their function is described in Table 2.1. An overview of the chemical structures of common types is located in Appendix A.

2.2 Lubricant Transformation

The lubricating oil on the top land is directly exposed to the harsh thermal environment of the combustion chamber as well as acidic byproducts of combustion. Due to high residence time shown in [45], additive packages lose effectiveness and allow deposits to form. Many physical effects such as vaporization, oxidation, shearing, also contribute to the breakdown and formation of deposits [3].

Calculations performed for this work, and in [34] show oil temperature fluctuations between 300°C and 400°C. Piston studies cite a single number around 350°C and combustion studies show crevice gas temperatures as high as 550°C [8, 41]. Studies [17] have shown that oxidation is the primary degradation mechanism related to carbon deposits. Others stress the importance of vaporization [12]. All show that temperature plays a very large role in the formation of deposits [31].

[1]Depressants lower the pour point, the temperature at which oil will flow, typically used as a measure of pumpability; see ASTM D97.

Type	Purpose
Antioxidants	Increase oxidation stability, reduce varnish formation, increase life
Detergents	Reduce or prevent deposit formation at high temperatures
Dispersants	Retard sludge formation by putting insoluble oxidation and combustion products in suspension
Corrosion Inhibitors	Protect bearing metal surfaces from corrosive action of acids and peroxides
Rust Inhibitors	Protect ferrous surfaces from moisture
Viscosity Index Improvers	Reduce sensitivity of viscosity to temperature
Depressants	Lower pour point
Foam Inhibitors	Prevent the formation of stable foam
Tribological Agents (Anti-wear)	Reduce wear on steel-steel contacts, increase oil film strength

Table 2.1: Summary of Typical Additive Groups [29, 9]

Theoretical work done in [12] concluded that lubrication oil vaporization is a key contributor to many problems, including the formation of deposits. Vaporization is an important part of this problem because as lighter species are removed from the oil, its physical properties change. [25] and [13] both describe how to model liner vaporization as a major contributor to oil consumption. The same approach can easily apply to vaporization from the top land. By applying a convective mass transport for species i, flux across the oil-gas interface is [26]:

$$m''_{e,i}(x,y,t) = g_{m,i}(x,y,t) \cdot (mf_{s,i}(x,y,t) - mf_{\infty}) \tag{2.1}$$

where we can define a mass transfer coefficient $g_{m,i}$ for component i across the mass fraction gradient at the oil-gas interface. The mass fraction of oil in the cylinder gases, mf_{∞}, is assumed to be close to zero. The mass fraction at the surface can be computed from the vapor pressure. Details of this calculation can be found in Section 3.5.

2.3 Modeling Framework

In theory, if one were to combine the mechanical and chemical processes of the engine, any engine property could be modeled. Unfortunately, not all engine operations are practical to precisely model. Attempts have been made, especially [11], [10] and [35] to combine numerical modeling with benchtop experiments to model engine operation.

The remaining problem to address is how to determine kinetic constants for reaction rates. Some experimental work has already compiled kinetic constants for molecules of interests for this project [4]. As is often the case in numerical modeling, this is a difficult task due to the sheer volume of reactions to consider, so we must consider a reduced set of equations. In addition to the quantity of reactions, there is also the problem of interactions between reactions and non-linear effects[2]. This work will not attempt to offer a solution to these problems, but simply set up an environment where those solutions can utilize the information gathered (temperatures, concentrations, and so on) by this work.

Though not applied to this problem yet, we can describe the general framework of a chemical simulation applied to this problem. The essential requirement for permitting future chemical reactions is a detailed description of the environment, which TLOTTS computes during the simulation.

[2]Synergies between additives are known, but there still exists some art to designing additive packages

Chapter 3

Numerical Modeling

3.1 Approach

The following sections will assume the reader is familiar with basic fluid mechanics and heat and mass transfer. In addition, it would likely be helpful to have some background in basic numerical methods and discretization schemes. For clarification purposes, typically a reminder of the form of certain numerical approximations will be repeated, but for many repeated applications, the intermediate steps may be skipped.

In addition, the computational algorithms described in the following section were selected for application to this specific set of problems and are not intended to be rigorous approaches for any CFD problem.

3.2 Coordinate System

For the rest of this document, the coordinate system defined in Figure 3-1 will apply. The computational domain (defined in Section 4.3.1 in more detail), will be in the x-y plane of the coordinate system shown. The top land-combustion chamber interface is at $y = 1$ and the top land-ring pack inferface is at $y = 0$.

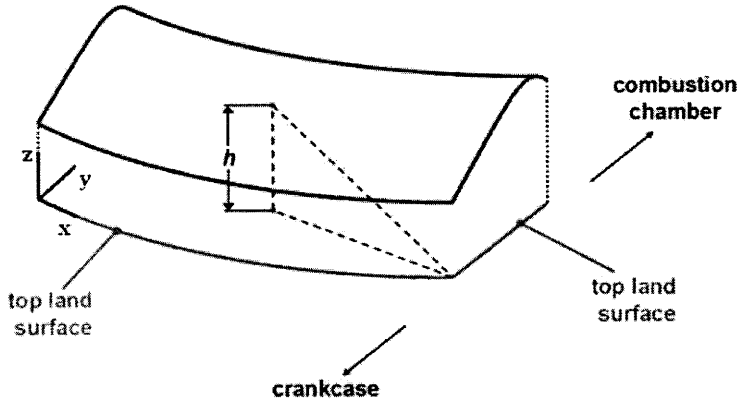

Figure 3-1: Coordinate System Modified from [34]

3.3 Navier-Stokes Solver

The governing equation for the conservation of momentum for fluids is the Navier-Stokes (Equation 3.1). This is a notoriously difficult equation to solve. Applying a lubrication assumption[1], that flow velocity in the z-direction may be neglected, and then a scaling analysis to eliminate terms, simplifies the equation.

$$\frac{D\vec{v}}{Dt} = -\frac{1}{\rho}\vec{\nabla}p + \nu\nabla^2\vec{v} \tag{3.1}$$

Finally, two boundary conditions are applied to the oil profile: (1) the no-slip condition and (2) gas shear must match oil shear at the interface. The derived conservative form, applied to this problem can be seen in Equation 3.2. The full derivation of this general equation can be found in [34]. Typical accelerations,a_p, as a function of crank angle can be seen in Figure ??

$$\frac{\partial}{\partial x}\left(\frac{1}{2}\frac{\mu_{gas}}{\mu_{oil}}\frac{\partial u_{gas}}{\partial z}\Big|_{z=h}h^2\right) + \frac{\partial}{\partial y}\left(-\frac{a_p}{3\nu}h^3 + \frac{1}{2}\frac{\mu_{gas}}{\mu_{oil}}\frac{\partial v_{gas}}{\partial z}\Big|_{z=h}h^2\right) + \frac{\partial h}{\partial t} = 0 \tag{3.2}$$

[1]Justified by length ratio $h/L << 1$. Characteristic values are 20 μm and 15mm, respectively.

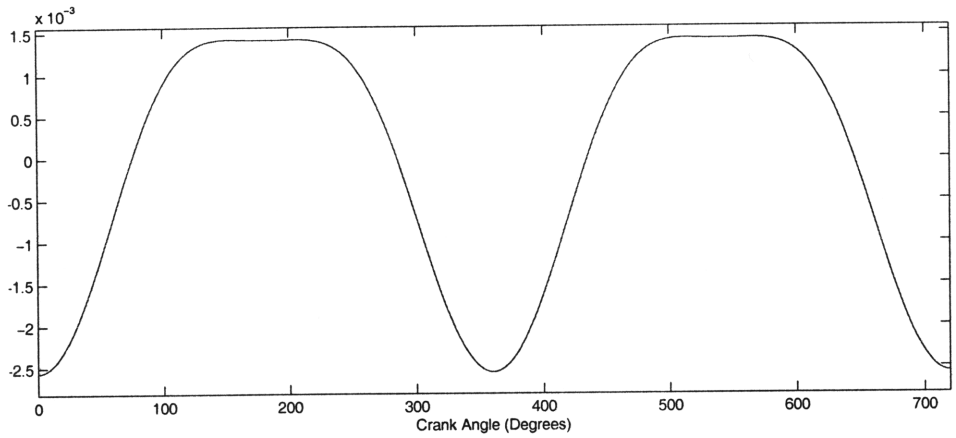

Figure 3-2: Typical non-dimensional accelerations seen by oil film

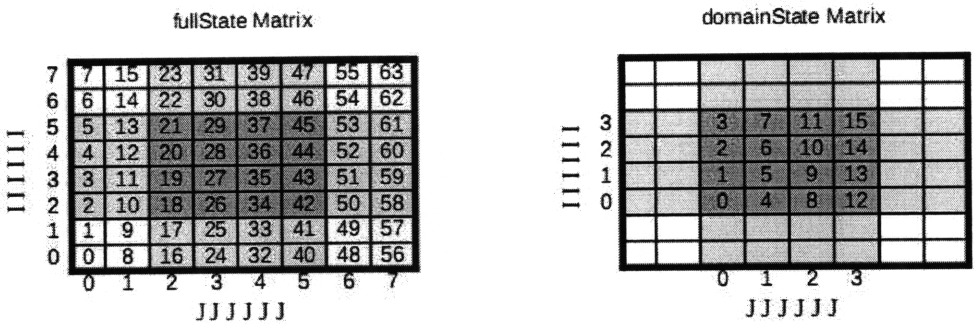

Figure 3-3: Full state grid showing ghost cells for Navier-Stokes solver

3.3.1 Boundary Conditions

The solver for the Navier-Stokes equation (3.2) places the ghost cells around the domain matrix to create a full state matrix as seen in Figure 3-3. Within these ghosts cells, the appropriate values are filled according to boundary conditions. There are two rows of boundary cells to compute higher derivatives. The white cells shown are not included in any computations.

3.4 General Transport Solver

This solver is used to describe movement of a scalar quantity under diffusive and convective sources. It can be used here to calculate the movement of mass concentrations

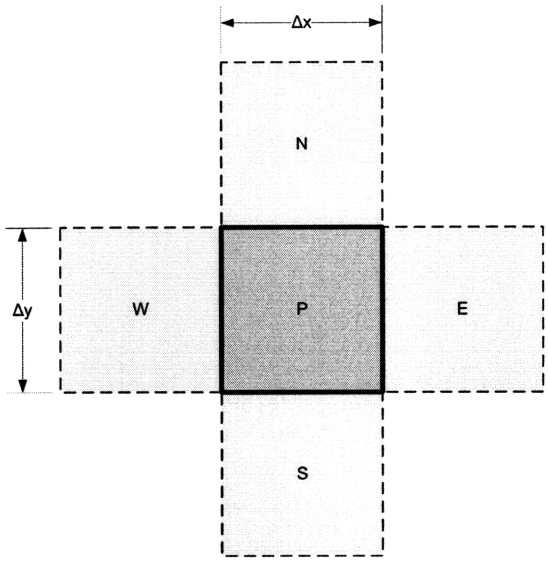

Figure 3-4: Neighboring node nomenclature for general transport equation

and energy (temperature). We'll take a modified 2d approach to this problem by only permitting fluxes through the x and y faces, and accounting for fluxes through the z faces by introducing addition boundary conditions. Both the thickness or height of each cell, h, and the velocity field, $\vec{u}$, are determined by the results of the Navier-Stokes solver.

3.4.1 Interior Nodes

The conservation law for transport of a scalar under the influence of unsteady flows is the general transport equation. Fortunately, the same equations and even the same discretization schemes can be used to model the transport of both the temperature field and concentration of species. Derivations will utilize a general parameter and coefficients and appropriate values for each parameter will be noted. A similar derivation can be found in [46].

Unsteady transport of a general parameter ϕ is given by:

$$\overbrace{\frac{\partial}{\partial t}(\rho\phi)}^{A} + \overbrace{\nabla \cdot (\rho\vec{u}\phi)}^{B} = \overbrace{\nabla \cdot (\Gamma \nabla\phi)}^{C} + \overbrace{S_\phi}^{D} \tag{3.3}$$

where the rate of change of ϕ (A) plus the flux of ϕ through the boundaries of the cell (B) is equal to the diffusive flux of ϕ through the boundary (C) plus an addition source and sink term (D). Clever readers may note that term (C) and (A) make Fick's Second Law of diffusion, where Γ is used here in place of D for the diffusion constant. For mass transport, the diffusion constants[2] are very low [18], and term (B) is orders of magnitude higher, so we can safely drop it. In the case of conduction when applied to thermal transport, for nearly all the input data that TLOTTS will see, terms (B) and (C) will be much larger than term (C) as well, but in the interest of robustness, we'll include the diffusion terms for Peclet numbers less than 2. For both the thermal and mass transport cases, Peclet number represents the ratio between convective and diffusive fluxes, where values over 2 are considered convection dominated transport.

To make use of the general transport equation, we'll need to develop it into a form useful for performing calculations. Writing the general case in three dimensions and expanding derivatives:

$$\begin{aligned} &\frac{\partial(\rho\phi)}{\partial t} + \frac{\partial(\rho\phi u)}{\partial x} + \frac{\partial(\rho\phi v)}{\partial y} + \frac{\partial(\rho\phi w)}{\partial z} \\ &\qquad = \frac{\partial}{\partial x}(\Gamma\frac{\partial\phi}{\partial x}) + \frac{\partial}{\partial y}(\Gamma\frac{\partial\phi}{\partial y}) + \frac{\partial}{\partial z}(\Gamma\frac{\partial\phi}{\partial z}) + S_\phi \end{aligned} \tag{3.4}$$

The thin film assumption enforces $w = 0$ and because our computational grid is only one cell thick in the z-direction, we'll lump that term into S along with our x and y boundary conditions. Assuming the function is local, to determine the value of ϕ_P at time $t + \Delta t$ we'll attempt to solve this equation and put it in the discretized form, where the new value of ϕ_P is equal to the old value of ϕ_P, the surrounding nodes, and any source terms:

$$a_P\phi_P = a_P^0\phi_P^0 + a_N^0\phi_N^0 + a_S^0\phi_S^0 + a_E^0\phi_E^0 + a_W^0\phi_W^0 + S_u \tag{3.5}$$

The values of the surrounding nodes are weighted by a factor a, which is determined

[2]For example, the self-diffusion constant for n-decane at 300°C is on the order of 10^{-9} m^2/s and scales logarithmically with the inverse of temperature

by the strength of the flux through the cell interface. The assumption of (3.5) is that the value of ϕ_P at time $t + \Delta t$ depends explicitly on the value of ϕ_P and the immediate surrounding nodes at time t. This explicit behavior is a consequence of the discretization decision and allows us to put all the terms from the previous time step (denoted as ϕ^0) on the right hand side of the equation. Like the solution to the Navier-Stokes equation, we'll apply a finite volume approach to discretize this equation. In typical fashion, we will integrate over the fluid volume and then over the time step from t to $t + \Delta t$:

$$\begin{aligned} &\overbrace{\int_{CV}\int_{t}^{t+\Delta t}\frac{\partial(\rho\phi)}{\partial t}dtdV}^{A} + \overbrace{\int_{t}^{t+\Delta t}\int_{A}\left(\frac{\partial(\rho\phi u)}{\partial x}+\frac{\partial(\rho\phi v)}{\partial y}\right)dAdt}^{B} \\ &= \overbrace{\int_{t}^{t+\Delta t}\int_{A}\left(\frac{\partial}{\partial x}(\Gamma\frac{\partial\phi}{\partial x})+\frac{\partial}{\partial y}(\Gamma\frac{\partial\phi}{\partial y})\right)dAdt}^{C} + \overbrace{\int_{t}^{t+\Delta t}\int_{CV}S_\phi dVdt}^{D} \end{aligned} \tag{3.6}$$

We'll treat the four terms in (3.6) separately in the following discussion. We'll apply an explicit scheme, evaluating fluid properties at time t and grid location P (unless otherwise noted) and allowing values to vary bilinearly[3] between nodes.

Expanding term (A) by applying Backward Differencing in time and applying the value of ϕ over the whole control volume[4]

$$\begin{aligned} \int_{CV}\int_{t}^{t+\Delta t}\frac{\partial(\rho\phi)}{\partial t}dtdV &= \rho\left(\frac{\phi_P^{t+\Delta t}-\phi_P^t}{\Delta t}\right)h_P\Delta t\Delta x\Delta y \\ &= \rho\left(\phi_P^{t+\Delta t}-\phi_P\right)\Delta x\Delta y h_P \\ &= (h\rho)_P\Delta x\Delta y\phi_P^{t+\Delta t}-(h\rho)_P\Delta x\Delta y\phi_P \end{aligned} \tag{3.7}$$

[3]Evaluating the value of ϕ_n on a constant grid width Δx to $\frac{\phi_N+\phi_P}{2}$

[4]Keep in mind because our control volume is 2.5D, the 3rd dimension will not cancel and the total volume for a cell P is $h_P\Delta x\Delta y$

Expanding the convection term (B) using an explicit time step:

$$\begin{aligned}
&\int_t^{t+\Delta t}\int_A \left(\frac{\partial(\rho\phi u)}{\partial x}+\frac{\partial(\rho\phi v)}{\partial y}\right)dAdt \\
&= \int_t^{t+\Delta t}\underline{[(\rho uA\phi)_e-(\rho uA\phi)_w]}dt+\int_t^{t+\Delta t}[(\rho vA\phi)_n-(\rho vA\phi)_s]dt \\
&= \{[(\rho uA\phi)_e-(\rho uA\phi)_w]+[(\rho vA\phi)_n-(\rho vA\phi)_s]\}^t\,\Delta t \\
&= \Delta t\Delta y\frac{(h\rho u)_e}{2}(\phi_E+\phi_P)-\Delta t\Delta y\frac{(h\rho u)_w}{2}(\phi_W+\phi_P) \\
&+\Delta t\Delta x\frac{(h\rho v)_n}{2}(\phi_N+\phi_P)-\Delta t\Delta x\frac{(h\rho v)_s}{2}(\phi_S+\phi_P)
\end{aligned} \tag{3.8}$$

Expanding the diffusive term (C) using Central Differencing[5] and an explicit time step:

$$\begin{aligned}
&\int_t^{t+\Delta t}\int_A \left(\frac{\partial}{\partial x}(\Gamma\frac{\partial\phi}{\partial x})+\frac{\partial}{\partial y}(\Gamma\frac{\partial\phi}{\partial y})\right)dAdt \\
&= \left\{\left[(h\Gamma\frac{\partial\phi}{\partial x})_n-(h\Gamma\frac{\partial\phi}{\partial x})_s\right]\Delta y+\left[(h\Gamma\frac{\partial\phi}{\partial y})_e-(h\Gamma\frac{\partial\phi}{\partial y})_w\right]\Delta x\right\}^t\Delta t \\
&= h_n\Gamma_n(\phi_N-\phi_P)\frac{\Delta t\Delta y}{\Delta x}-h_s\Gamma_s(\phi_P-\phi_S)\frac{\Delta t\Delta y}{\Delta x} \\
&+h_e\Gamma_e(\phi_E-\phi_P)\frac{\Delta t\Delta x}{\Delta y}-h_w\Gamma_w(\phi_P-\phi_W)\frac{\Delta t\Delta x}{\Delta y}
\end{aligned} \tag{3.9}$$

Finally, expanding the source term (D):

$$\begin{aligned}
\int_t^{t+\Delta t}\int_{CV} S_\phi dV dt &= \left\{\bar{S}\Delta x\Delta y\Delta h\right\}^t\Delta t \\
&= S_u+S_p\phi_P
\end{aligned} \tag{3.10}$$

To get into the form of (3.5) we'll move the previous time step terms to the right

[5]For example: $\frac{\partial\phi}{\partial x}|_n \approx \frac{\phi_N-\phi_P}{\Delta x}$

hand side (subtracting (B) and the second term of (3.7)) and group terms:

$$
\begin{aligned}
&(h\rho)_P \Delta x \Delta y \phi_P = \\
&\left[(h\rho)_P \Delta x \Delta y - h_n \Gamma_n \frac{\Delta t \Delta y}{\Delta x} - h_s \Gamma_s \frac{\Delta t \Delta y}{\Delta x} - h_e \Gamma_e \frac{\Delta t \Delta x}{\Delta y} - h_w \Gamma_w \frac{\Delta t \Delta x}{\Delta y}\right] \phi_P^0 \\
&+ \left[-\frac{(h\rho u)_e}{2} \Delta t \Delta y + \Delta t \Delta y \frac{(h\rho u)_w}{2} - \Delta t \Delta x \frac{(h\rho v)_n}{2} + \Delta t \Delta x \frac{(h\rho v)_s}{2}\right] \phi_P^0 \\
&+ \left[h_n \Gamma_n \frac{\Delta t \Delta y}{\Delta x} - \Delta t \Delta x \frac{(h\rho v)_n}{2}\right] \phi_N^0 \\
&+ \left[h_s \Gamma_n \frac{\Delta t \Delta y}{\Delta x} + \Delta t \Delta x \frac{(h\rho v)_s}{2}\right] \phi_S^0 \\
&+ \left[h_e \Gamma_n \frac{\Delta t \Delta x}{\Delta y} - \Delta t \Delta y \frac{(h\rho u)_e}{2}\right] \phi_E^0 \\
&+ \left[h_w \Gamma_n \frac{\Delta t \Delta x}{\Delta y} + \Delta t \Delta y \frac{(h\rho u)_w}{2}\right] \phi_W^0
\end{aligned}
\tag{3.11}
$$

The form of (3.11) should begin to look somewhat like (3.5). The last step is to define the coefficients of ϕ_P, ϕ_P^0, ϕ_N^0, etc by the familiar form a_P, a_P^0, a_N^0, etc. For clarity, we will define an intermediate value, F_k, the convective flux coefficient through face k, and D_k, the diffusive flux coefficient through face k. Using these definitions, we can build the following table:

	N	S	E	W
F	$(h\rho v)_n \Delta x$	$(h\rho v)_s \Delta x$	$(h\rho u)_e \Delta y$	$(h\rho u)_w \Delta y$
D	$\Gamma_n h_n \Delta y / \Delta x$	$\Gamma_s h_s \Delta y / \Delta x$	$\Gamma_e h_e \Delta x / \Delta y$	$\Gamma_w h_w \Delta x / \Delta y$

Table 3.1: Summary of Intermediate Flux Coefficients

For evaluating the value of the coefficients we'll utilize the Hybrid Differencing Scheme (HDS) as our Peclet numbers range above and below 2. The hybrid scheme reduces Central Difference Errors with highly convective flows by ignoring the diffusion term. For $Pe > 2$, it reverts to an Upwind Differencing Scheme (1st Order). For $Pe < 2$, HDS uses a Central Differencing Scheme (2nd Order). This is accomplished by assigning the values of the coefficients a_P^0, a_N^0, etc according to Table 3.4.1.

Coefficient	Value
a_P	$\rho\Delta x\Delta y\Delta h/\Delta t$
a_P^0	$a_P - (a_N^0 + a_S^0 + a_E^0 + a_W^0) - \Delta F + S_p$
a_N^0	$max(-F_N, D_N - F_N/2, 0)$
a_S^0	$max(+F_S, D_S + F_S/2, 0)$
a_E^0	$max(-F_E, D_E - F_E/2, 0)$
a_W^0	$max(+F_W, D_W + F_W/2, 0)$
ΔF	$F_N - F_S + F_E - F_W$

Table 3.2: Evaluation of Flux Coefficients

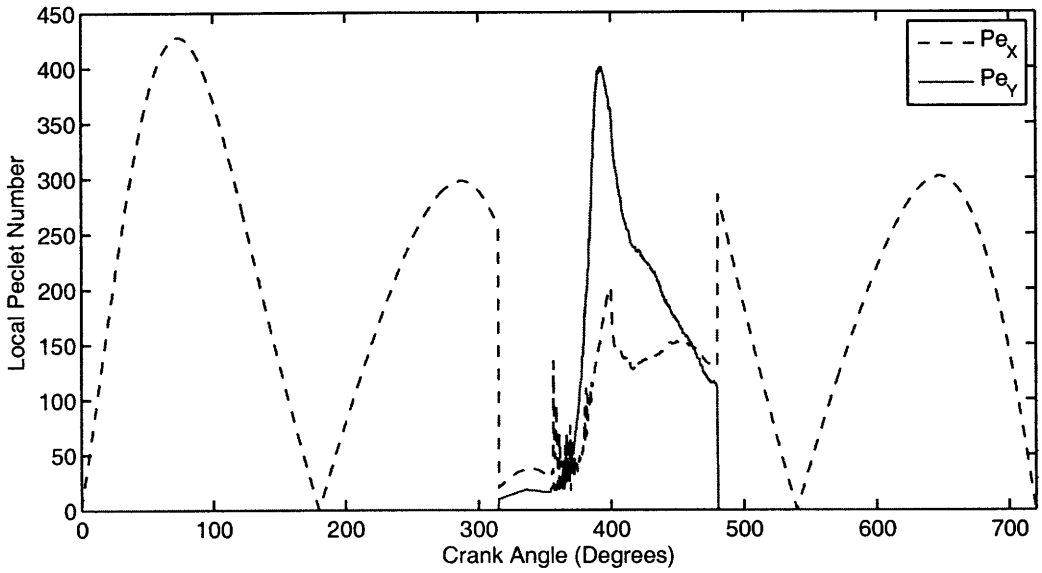

Figure 3-5: Typical Local Peclet Numbers

We can find the value at the next time step $t + \Delta t$ explicitly by:

$$\phi_P = \frac{\phi_P^0 a_P^0 + \phi_N^0 a_N^0 + \phi_S^0 a_S^0 + \phi_E^0 a_E^0 + \phi_W^0 a_W^0 + (S_u + S_p \phi_P^0)}{a_P} \tag{3.12}$$

To find the values of S_u and S_p, we'll have to apply boundary conditions.

3.4.2 Boundary Conditions

Inevitably, the most challenging computational question is how to treat boundary conditions. This problem will require mixed boundary conditions[6]: Dirichlet, Neumann, periodic, and Cauchy. The following sections will describe the computational boundaries, what the physical boundary conditions are, and what numerical boundary condition the model will apply.

Periodic Boundary Conditions

Periodic boundary conditions are often applied in cases of geometric or computational symmetry, especially when it's prudent to reduce the degrees of freedom of a calculation by subdividing the physical space. In this case, the piston's axisymmetric geometry combined with the fuel nozzles (which in our simulated engine, number 5) suggests division into 5 axisymmetric wedges and application of a periodic boundary condition across them.

For the general transport equation (3.5), the specific implementation of these boundary conditions is described in the following sentences. As the solver loops through the computational nodes, a function gives the number of the surrounding nodes, usually denoted as *North*, *South*, *East*, or *West*. If the function determines that the current node is a boundary node (by looking at whether the node's j coordinate is 0 or J), it will return the opposite node. For instance, for a node with nodal coordinates (i, 0) the function will return (i, J) for the *West* node. Similarly, when computing using more than the directly adjacent node, the function will return (i, $J-1$) when asked for the (i, -2) node (as required to compute higher derivatives). Because now the solver will now have the correct value to apply the boundary condition, no further steps are required (and no modifications to the main algorithm).

[6]See [44] for a general treatment of these conditions or [46] for how it pertains to fluid dnyamics.

Ring Pack and Combustion Chamber Boundary Conditions

The ring pack provides the south and the combustion chamber provides the north boundary condition. Experimentally, it was found that the ring pack tends to accumulate oil, and provide a pumping action as the ring flutters in the groove [45]. During the cycle, however, we may experience both inflow and outflow across these boundaries. They will be treated separately.

Inflow Conditions: This is the simpler of the two cases. When inflow conditions are detected, a set value is used (a Dirichlet condition). For the combustion chamber, this is typically zero, and for the ring pack, this is user configurable, but typically around the value of the characteristic thickness.

Outflow Conditions: The same approach is again applied to both boundaries for the outflow condition. To allow for proper upwinding, the boundary condition is extrapolated from the interior nodes.

Piston Surface and Gas Surface Boundary Conditions

These are both user supplied Dirichlet boundary conditions. Gas temperature comes from gas flow data, and piston temperature comes from user supplied piston data. Each can be a function of time and space. If the TLOTTS calculations were integrated into the combustion and piston temperature calculations, then it would be appropriate to consider applying flux boundary conditions, modeling the oil as a resistive element to the transfer of heat from the hot combustion gases to the (often oil-cooled) piston as shown in [48]. In addition, once the chemical model can accurately predict formation rates of carbon deposits, their thermal resistance should be added between the top land oil and piston surface, as seen in [36].

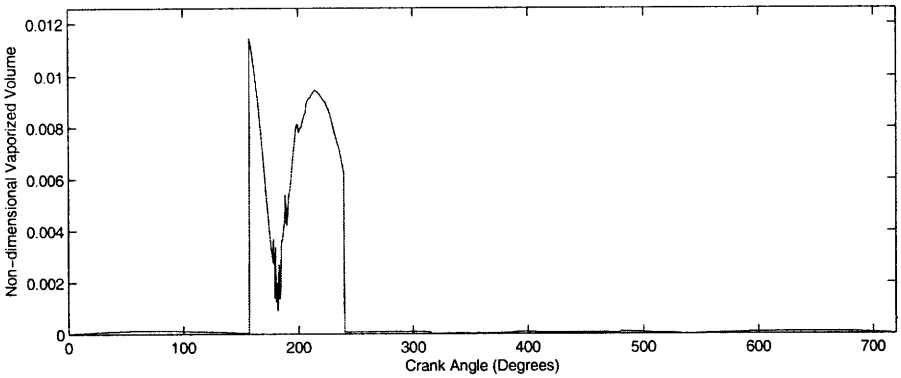

Figure 3-6: Typical vaporization volume for a cycle

3.5 Vaporization

As mentioned in Section 2.2, an effective way to model vaporization is using a mass transfer analogy shown in Equation 3.13.

$$m''_{e,i}(x,y,t) = g_{m,i}(x,y,t) \cdot (mf_{s,i}(x,y,t) - mf_{\infty}) \tag{3.13}$$

We will assume that the quantity of oil components in the cylinder gases is negligible, so all that is left to determine is the mass transfer coefficient $g_{m,i}$ and the mass fraction of oil vapor at the oil-gas interface $mf_{s,i}$. Vaporization primarily occurs when exposed to the hot combustion gases as seen in a typical case in Figure 3-6.

3.5.1 Mass Transfer Coefficient

Extending the heat transfer analogy, we can use the Nusselt-Reynolds-Prandtl correlation [26] (Equation 3.14) to create the Sherwood-Reynolds-Schmidt relation (Equation 3.15).

$$Nu = a \cdot Re^d \cdot Pr^e \tag{3.14}$$

$$Sh = a \cdot Re^d \cdot Sc^e \tag{3.15}$$

where

$Nu = \frac{hL}{k}$	Nusselt Number	L	Characteristic Length
$Re = \frac{vL}{\nu}$	Reynolds Number	V	Characteristic Velocity
$Pr = \frac{\nu}{\alpha}$	Prandtl Number	k	Thermal Conductivity
$Sh = \frac{g_m L}{\rho D_{ab}}$	Sherwood Number	ν	Kinematic Viscosity
$Sc = \frac{\nu}{D_{ab}}$	Schmidt Number	α	Thermal Diffusivity
		ρ	Density
		D_{ab}	Binary Diffusion Coefficient

Like most relations, this one has a few assumptions; (1) the vaporization rate must remain a low mass transfer rate process and (2) the temperature of the oil film must not exceed the boiling point of any of the species because a fundamental feature of Equation 3.13 is that it is a diffusion limited process[7]. Using experimental results from [5], [25] was able to come up with suggested values of constants in Equations 3.14 and 3.15:

$a = 0.035$ to 0.13

$d = 0.7$ to 0.8

$e = 0.667$

Rearranging Equation 3.15 to solve for the mass transfer coefficient:

$$g_m = a \cdot \rho \cdot L^{d-1} \cdot \nu^{e-d} \cdot D_{ab}^{1-e} \cdot V^d \tag{3.16}$$

TLOTTS defines density and viscosity as functions of temperature and location[8], so the only remaining property to discuss here is the binary diffusion constant. [25] shows that the binary diffusion constant can be approximated by methods outlined in [32] using a temperature-pressure correction.

[7]Boiling is an energy limited process.

[8]User provided data.

3.5.2 Mass Fraction at Oil-Gas Interface

The mass fraction of oil species at the oil-gas interface can be estimated by

$$mf_{s,i}(x,y,t) = \left(\frac{\overline{mf_{l,i}(x,y,t)} P_{v,i}(T_s)}{P_{cyl}(t)} \right) \frac{MW_i}{MW_\infty} \tag{3.17}$$

where $\overline{mf_{l,i}(x,y,t)}$ is the local instantaneous mole fraction of species i in the liquid oil film, $P_{v,i}(T_s)$ is the vapor pressure of species i at temperature T_s at the surface of the film. TLOTTS calculates each of these values. MW_i is the molecular weight of species i as determined in Section 3.5.3. MW_∞ is the average molecular weight of the gas, which because we've assumed mf_∞ is zero, MW_∞ is taken to be the molecular weight of air.

3.5.3 Evaluating Oil Properties

For the simple model, engine oil is modeled as several different paraffin hydrocarbon components with different liquid-phase mass fractions and boiling points. From the distillation curve of a particular oil or fuel, it is possible to discretize the curve into any number of species of mass fraction X with a boiling point equal to the temperature at which it vaporizes as shown Figure 3-7 [13, 40, 49].

From the boiling point, a polynomial created from tabulated data described in [47] can be used to find the molecular weight of a pure paraffin hydrocarbon [25]. Applying the Antoine equation (3.18) using constants found in [47], an approximation of vapor pressure can be determined.

$$log_{10}(P_v) = A - \frac{B}{C + T_s} \tag{3.18}$$

Now that vapor pressure and molecular weight of each species has been determined, it is possible to compute the mass flux due to vaporization and integrate this back within the model as a mass sink from the top land.

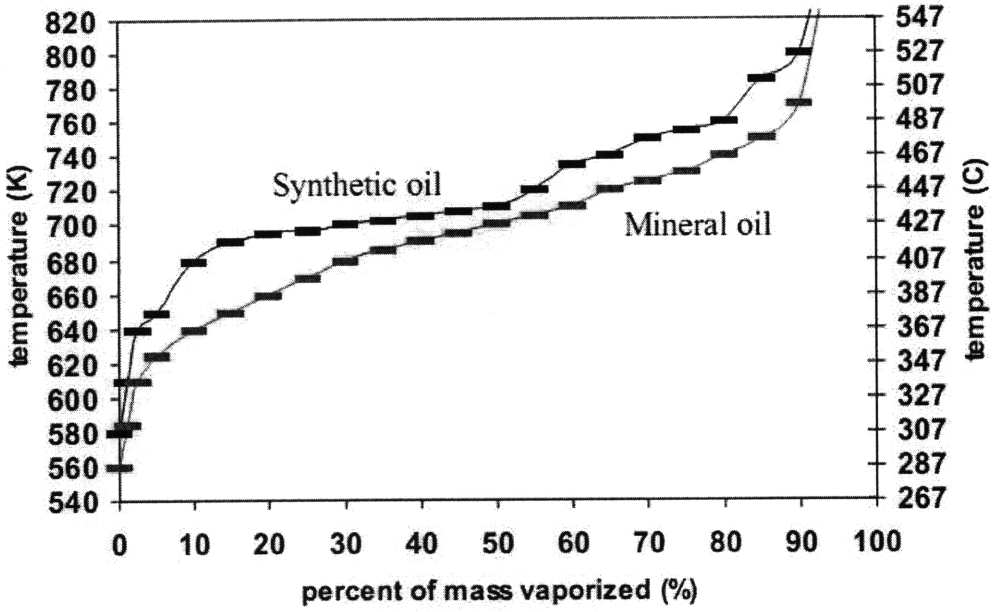

Figure 3-7: Discretization of mineral and synthetic oils for simulation [13]

THIS PAGE INTENTIONALLY LEFT BLANK

Chapter 4

Implementation and Results

This section serves as a more detailed description of the simulation steps as well as an incomplete user guide.

4.1 General Framework

TLOTTS consists of three stages: preprocessing, simulation, and post-processing. Code was prototyped in MATLAB and then solvers were written in compiled C using gcc4.2.4 under Linux or PellesC under Windows using MATLAB's built in `mex` function.

A single case can be run by typing `master('configuration.txt')` where 'configuration.txt' is a text input file defining the various simulation properties (CFD data location, time step, grid size), the engine properties (rpm, piston geometry), and various oil properties (viscosity, density).

Or, a batch run can be defined by a spreadsheet matching the format in Figure 4-1 and executed by `batchRun('batchfile.xls')`. If a parameter is not set by the batch file, it will be set according to the default configuration file 'TLOTTS.txt', which is also used if no configuration file is supplied when executing `master`.

Once a simulation run is started, the status will be output to the display, as well as

	A	B	C	D	E	F	G	H
1	baseGasDataFolder	/home/tgrimley/Documents/Sloan Auto/Gas Flow Data/						
2		Numerical Parameters				Top Land Geometry		
3	gasData	radJ	axil	tStep_deg	maxCrankAngle_deg	heightTopland_m	diameterTopland_m	tlClearance_m
4	Phase1-1	120	80	0.5	504000	0.02	0.1302	0.00050
5	Phase1-2	120	80	0.5	504000	0.015	0.1302	0.00067
6	Phase1-3	120	80	0.5	504000	0.01	0.1302	0.00100
7	Phase1-4	120	80	0.5	504000	0.005	0.1302	0.00200
8	Phase2-1	120	80	0.5	504000	0.005	0.1302	0.00270
9	Phase2-2	120	80	0.5	504000	0.01	0.1302	0.00130
10	Phase2-3	120	80	0.5	504000	0.015	0.1302	0.00089
11	Phase2-4	120	80	0.5	504000	0.02	0.1302	0.00067
12	Phase3-1	120	80	0.5	504000	0.005	0.1302	0.00160
13	Phase3-2	120	80	0.5	504000	0.01	0.1302	0.00067
14	Phase3-3	120	80	0.5	504000	0.015	0.1302	0.00045
15	Phase3-4	120	80	0.5	504000	0.02	0.1302	0.00034

Figure 4-1: Example of batch run spreadsheet

logged in the results directory. Each time a simulation is run, a string is generated to identify the data set. The string is created from concatenating the input file name and current date and time[1].

4.2 Data Structures

There are two classes of data structures used throughout TLOTTS: state variables and structs. In general, structs will be set once at the start of a simulation, and state variables will change throughout the simulation. Structs which change during the simulation will be noted in the following sections.

4.2.1 State Variables

State variables describe the current state of the simulation. In TLOTTS there is one state variable for time, tCAD, and 4 state matrices (listed in Table 4.1) for physical parameters. Each matrix is at least of dimensions [I x J x 2], which contain values at grid location (i, j) and at time step t or $t + \Delta t$. At the end of each time step, TLOTTS moves the data from the `(:,:,2)` position into the `(:,:,1)` position for the next time step. These are global variables available to any function or subfunction

[1]Note that his string is not *unique* and running two instances of MATLAB and the same batch run can create collisions. Avoid doing this.

Name	Description	Units
hMatrix	Oil film thickness	Dimensionless
tMatrix	Temperature	Kelvin
cMatrix	Composition fraction, adds a 4th dimension to size [I x J x 2 x nSpecies]	Dimensionless
mMatrix	Amount of species, adds a 4th dimension to size [I x J x 2 x nSpecies]	Moles

Table 4.1: Description of TLOTTS state matrices

of the program, so future users must note where in the time step they make changes to these variables.

During chemical reactions, vaporization, or mixing, the quantity of oil on the top land is converted between these different forms by application of the oil's physical properties. For example, using density of an incompressible fluid such as oil, one can convert between mass and volume.

4.2.2 Structs

In addition to the state variables, there are also structs which define configuration settings as well as certain derived properties (viscosity, density, etc) which are functions of space, time, or temperature. These structs are defined in Table 4.2.

Name	Children	Description
prg	version copyright lastUpdated title	Contains information about the program
grid	tstar xstar ystar zstar ustar vstar wstar x_width y_width delta_x delta_y rclose FVxdomainlite FVydomainlite FVxdomain FVydomain betadomainx betadomainy gammadomainx gammadomainy oilAddMatrix	Contains computational grid description and non-dimensional conversions
shear	gasFlowAxial gasFlowCirc gasFlowCAD gasFlowTemp	Contains re-gridded gas flow and gas temperature data
piston	theta accel vel	Contains pre-computed instantaneous piston velocity and acceleration
sim	(Confidential)	Contains per timestep computed properties and time-averaged properties

Table 4.2: Description of TLOTTS struct variables

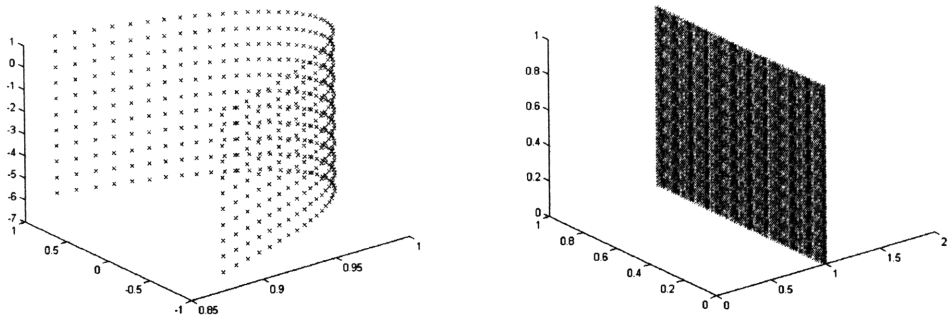

(a) (b)

Figure 4-2: TLOTTS' physical (a) and computational (b) domains.

4.3 Preprocessing

One of the design goals of TLOTTS was to improve performance of the simulation to make running parametric studies feasible. To this end, some quantities which do not change from cycle to cycle are precomputed and their values placed into a variable.

4.3.1 Initializing the Computational Domain

The first step in any simulation relying on a computational grid is to define the nodal points and a translation between nodal coordinates and physical or geometric coordinates. Fortunately, the physical domain (the top land of the piston) is a nearly rectangular coordinate system. TLOTTS' grid is normalized to height and width dimensions of [1,1] (shown in Figure 4-2). The changing grid depth is normalized to a characteristic[2] (user-configurable) depth of 20 μm.

4.3.2 Preallocating Variables

Preallocation variables is a required technique in most compiled languages and a good practice in scripted languages like MATLAB. Huge gains in speed come from

[2]A typical film depth of 20-30 μm was found in experimental studies [45].

preallocating the state variables and various other values before starting the simulation [20, 37]. This also helps mitigate some of the problems of memory management in MATLAB. All variables used in simulation are initialized before the simulation begins.

4.3.3 Importing CFD Data

Gas flow velocity data can be taken from many sources, often applying entirely different grids and computational methods. For this reason, TLOTTS must translate the velocity data into the regular grid that TLOTTS utilizes for calculations. This must be done efficiently because there are often thousands of data points that must be interpolated many times at each time step. An efficient way of calculating these interpolations is to precompute a Delaunay Triangulation and apply the same triangulation to each time step, and then interpolate linearly between time steps.

Delaunay Triangulations

Delaunay triangulations are used to generate well-behaved unstructured meshes for interpolation[3]. Refinement refers to the process of producing a new mesh with a larger number of smaller triangles. There is a MATLAB function that will compute this for us, which is based on the algorithm described in [6], but others exist [43].

In our case, we apply the Delaunay triangulation to refine our mesh comprising of data points from the unstructured gas flow data file to a mesh comprising of regular points describing our own computational domain. This has the benefit of fixing small errors in translation between polar and Cartesian coordinates. A good mesh can be seen in Figure 4-3 which corrects for small errors in a nearly uniform grid.

[3] A full description of this approach is outside the scope of this work; please consult [43] or [6] or Chapter 9 of [16].

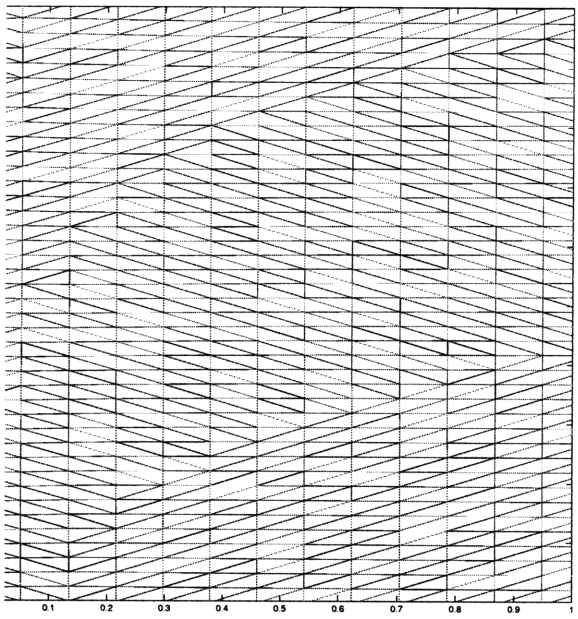

Figure 4-3: Delaunay generated mesh from imported gas flow data

Temporal Interpolation

Temporal interpolation is merely a point-by-point linear interpolation between time t_0 and t_1 according to the equation. For instance, to find the value of the parameter χ at time t_a such that $\epsilon[t_0, t_1]$:

$$\chi|_{t_a} = \chi_0 + (t_a - t_0)\frac{\chi_1 - \chi_0}{t_1 - t_0} \tag{4.1}$$

4.4 Post-Processing

Once the simulation registers cyclical convergence[4], it will run one more cycle and capture full data at each step, outputting user defined plots.

The data is saved to disk, and bulk parameters are output to a summary file which is useful for comparing runs directly. The film thickness and temperature data is saved to images, such as shown in Figure 4-4, for each CAD. Movies can also be created

[4]This metric is difficult to determine exactly. The current solution monitors rate of change of the mean cyclical values volume and temperature to look for convergence (1% change).

which stitch these plots together and help produce an intuitive understanding.

4.5 Typical Results

This next section will demonstrate some of the characteristics of typical simulations. Input gas flow was from a CFD simulation of the combustion process from a power cylinder design several years old, with steady state operation at 1500 rpm. Convergence of film thickness and film temperature (seen in Figures 4-5 and 4-6, respectively), is typically achieved in a few hundred cycles. Mean film temperature appears to converge faster in this example. These values can be seen moving between maximum and minimum cyclical values but that the base amplitude reaches a constant value. Temperature distributions (shown in Figure 4-4) typically inversely follow thickness; that is, where the film is thin, temperatures tend to be higher.

A combination of high gas velocities and a thin conductive film is favorable for heat transfer to the film. Similarly, high temperatures and high gas velocities during the combustion reaction rapidly increases the rate of vaporization, as shown previously in Figure 3-6. The top middle of the piston, seen as the sloping plains seen between 0.2 and 0.8 normalized width, has a thinner film with a higher temperature. This area approximately matches that of the fuel spray, and as the combustion flame expands it flows over the top land and parts the oil in the center area. The magnitude of oil flows in the axis of the piston is typically 100 times greater than that of oil flows around the circumference of the piston. Considering the input forces to the oil flow, this is to be expected, because as can be seen in Equation 3.2 gas flows are the only source of force in the circumferential direction.

The last feature to note in these results is the propagation of a wave front as seen in Figure 4-7. The shock capturing algorithms described in [34] can be seen put to good use as the front moves half-way across the domain from top to bottom. As one might imagine, during these types of flow, heat transfer is overwhelming dominated by convection as previously noted in Figure 3-5.

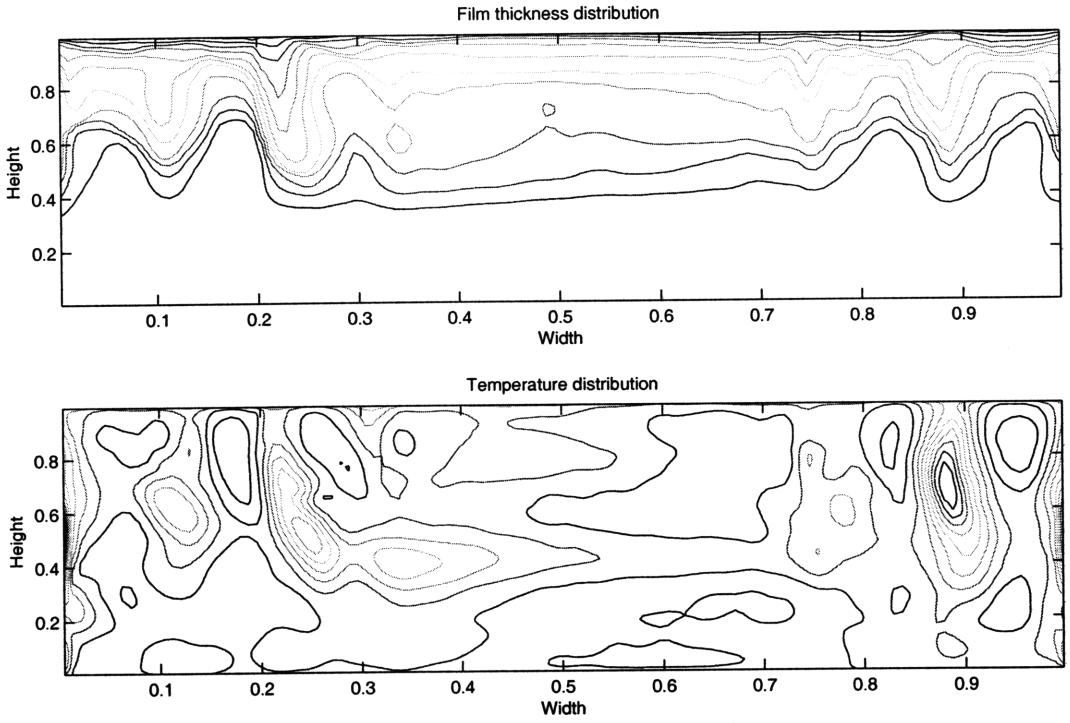

Figure 4-4: Typical film and temperature distributions

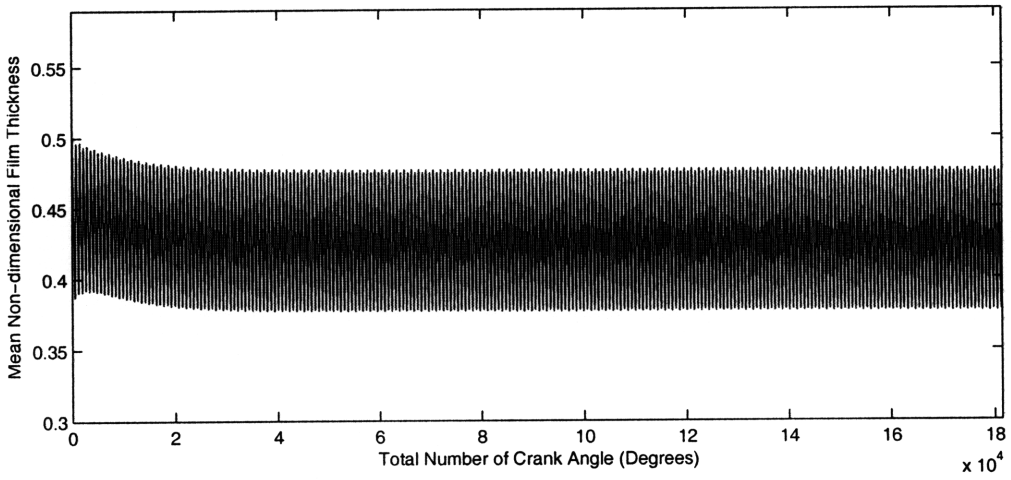

Figure 4-5: Film thickness convergence

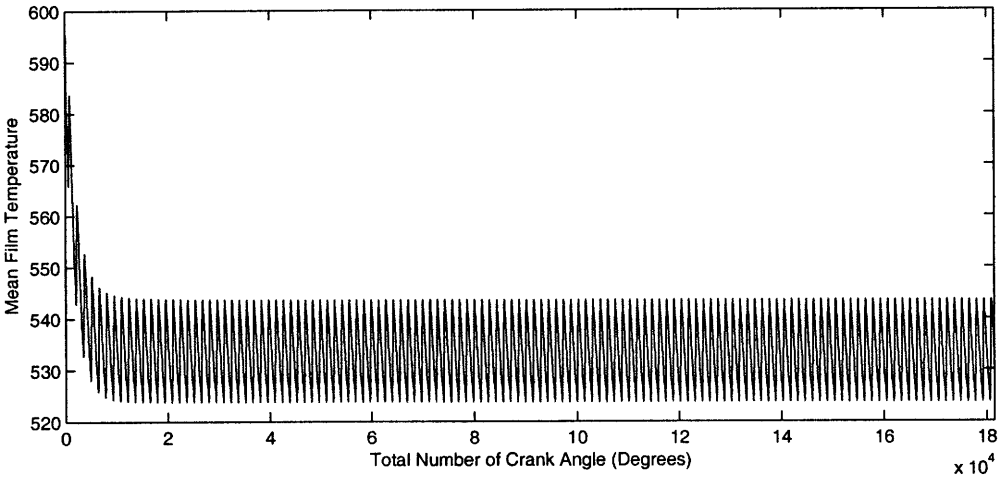

Figure 4-6: Film temperature convergence

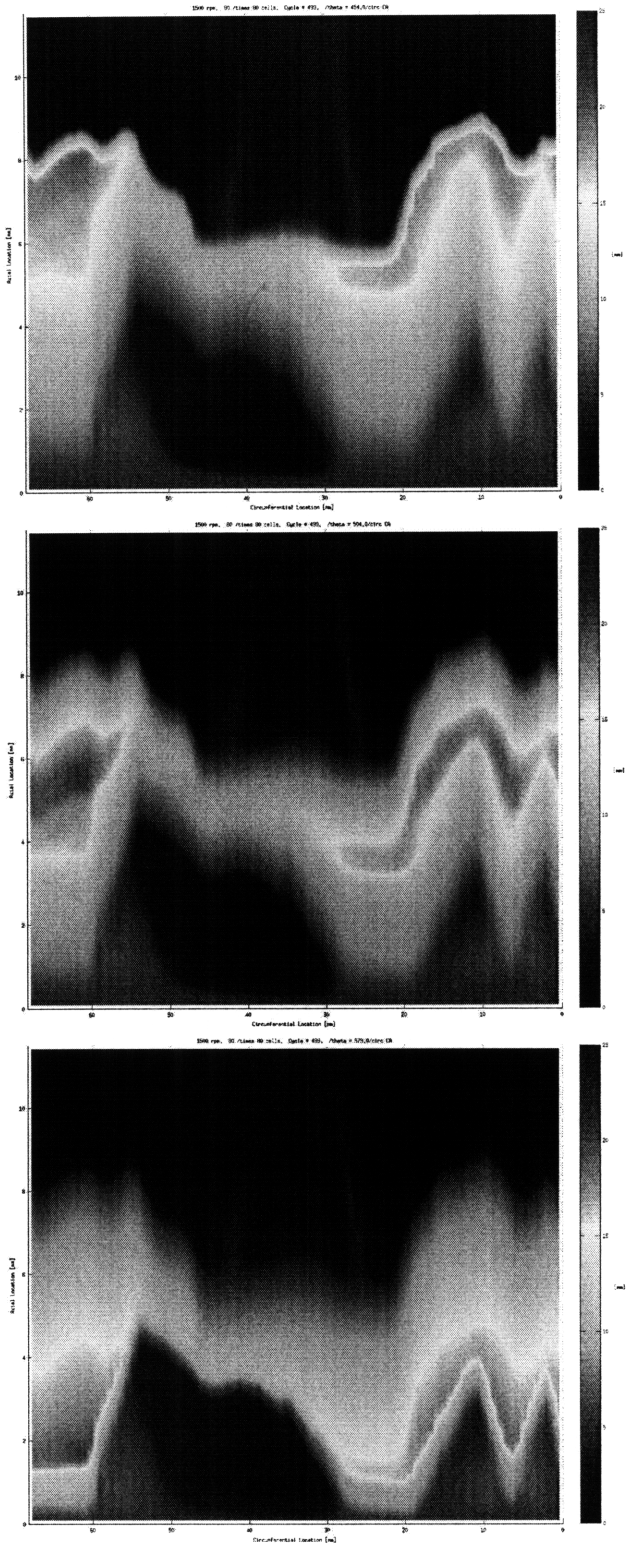

Figure 4-7: Movement of a film distribution through a cycle

4.6 Summary

A key objective of this work mentioned in Section 1.2 was to create a *fast* simulation to run to convergence. By paying careful attention to data structures and computation techniques, the simulation is able to achieve over 30 CAD / second[5] on a Intel Pentium Dual Core processor E2140 (1.60GHz,800MHz FSB) with 3GB RAM on Ubuntu 8.04 LTS and MATLAB R2008a. Slightly faster results on an Intel Pentium Quad Core Q6600 (2.4GHz,1066MHz FSB) with 8GB RAM on Windows Vista x64 SP1 and MATLAB R2008a. Although no tests were undertaken to confirm, this suggests the simulation is I/O limited rather than CPU limited and could benefit from porting the code from MATLAB to C.

The other goals, of course, are to create an *accurate* and *useful* simulation. To verify this result requires validation by some means. Current work is under way to statistically validate the conclusions drawn by simulation runs and correlate them with limited experimental data. By validating the simulation in this way it creates a useful tool with which to predict carbon deposit formation without the long lead time experiments and with comparatively little cost.

4.7 Future Work

As alluded to throughout, the key missing feature from this work is a full chemical model. This was impractical to implement at this stage due to a large uncertainty in the key chemical reactions and full theoretical knowledge of degradation of the lubrication oil. Fortunately, the results of an unrelated chemistry study predicting the degradation of oil can easily be combined with the current simulation to provide increased knowledge of the carbon formation process.

[5]Real time seconds, not computational seconds.

Bibliography

[1] Council directive on the approximation of the laws of the member states relating to measures to be taken against air pollution by gases from positive-ignition engines of motor vehicles. *Official Journal of 20 March 1970*, pages 1–22, 1970.

[2] 108th Congress of the United States. Clear air act, 2004. Available at `http://www.epa.gov/air/caa/`.

[3] A. Alizadeh and D. Trimm. The formation of deposits from oil under conditions pertinent to diesel engine pistons. *J. Chem. Tech. Biotechnol.*, 35A:291, 1985.

[4] D. L. Allara and R. Shaw. A compilation of kinetic parameters for the thermal degradation of n-alkane molecules. *J. Phys. Chem. Ref. Data*, 9(3):523–559, 1980.

[5] D. N. Assanis and J. B. Heywood. Development and use of computer simulation of the turbocompounded diesel system for engine performance components heat transfer studies. *SAE Technical Paper Series*, 1986.

[6] C. B. Barber, D. P. Dobkin, and H. T. Huhdanpaa. The quickhull algorithm for convex hulls. *ACM Transactions on Mathematical Software*, 22(4):469–483, Dec 1996.

[7] E. Bardasz, D. Mackney, N. Britton, G. Kleinschek, K. Olofsson, I. Murray, and A. Walker. Investigations of the interactions between lubricant-derived species and aftertreatment systems on a state-of-the-art heavy duty diesel engine. *SAE Technical Paper Series*, 2003.

[8] P. J. Burnett. Relationship between oil consumption, deposit formation and piston ring motion for single-cylinder diesel engines. *SAE Technical Paper Series*, 1992.

[9] A. J. Caines, R. F. Haycock, and J. E. Hillier. *Automotive Lubricants Reference Book*. SAE International, 2nd edition, 2004.

[10] C. Chen and S. M. Hsu. A chemical kinetics model to predict diesel engine performance. part ii. bench-test procedures. *Tribology Letters*, 14(2):91–97, February 2003.

[11] C. Chen and S. M. Hsu. A chemical kinetics model to predict lubricant performance in a diesel engine. part i: Simulation methodology. *Tribology Letters*, 14(2):83–90, February 2003.

[12] Y. Cho. Modeling engine oil vaporization and transport of the oil vapor in the piston ring pack of internal combustion engines. Master's thesis, Massachusetts Institute of Technology, 2004. Available at `http://dspace.mit.edu`.

[13] Y. Cho and T. Tian. Modeling engine oil vaporization and transport of the oil vapor in the piston ring pack of internal combustion engines. *SAE Technical Paper Series*, 2004.

[14] M. Covitch, D. Gundic, and R. Graf. Microstructure of carbonaceous diesel engine piston deposits. *STLE Journal*, 44(2):128, 1998.

[15] J. M. C. Pinto da Costa, L. Sarkisov, N. A. Seaton, and R. F. Cracknell. Adsorption-based structural characteristics of combustion chamber deposits. *SAE International*, 2009.

[16] M. de Berg, O. Cheong, M. van Kreveld, and M. Overmars. *Computational Geometry: Algorithms and Applications*. Springer-Verlag, 3rd edition, 2008.

[17] M. Diaby, M. Sablier, A. Le Negrate, M. El Fassi, and J. Bocquet. Understanding carbonaceous deposit formation resulting from engine oil degradation. *Carbon*, 47(2):355 – 366, 2009.

[18] D. C. Douglass and D. M. McCall. Diffusion in paraffin hydrocarbons. *J. Phys. Chem.*, 62(9):1102–1107.

[19] E. Durak and F. Karaosmanoglu. Using of cottonseed oil as an environmentally accepted lubricant additive. *Energy Sources*, 27(13):611–625, 2004.

[20] P. Gestruer. Writing fast matlab code. 2004.

[21] W. A Givens, W. H. Buck, A. Jackson, A. Kaldor, A. Hertzberg, W. Moehrmann, S. Muller-Lunz, N. Pelz, and G. Wenninger. Lube formation effects on transfer of elements to exhaust after-treatment system components. *SAE Technical Paper Series*, 2003.

[22] R. Gligorijevic, J. Jevtic, and D. J. Borak. Engine oil contribution to diesel exhaust emissions. *J. Synthetic Lubrication*, 23(1):27–38, 2006.

[23] H. Hirabayashi, K. Kiryu, A. Yoshino, and T. Koga. Electro-chemical investigation of deposit formation on mechanical seal surfaces for diesel engine coolant pumps. In W. J. Bartz, editor, *Engine Oils and Automotive Lubrication*, pages 779–793. Expert Verlag GmbH., 1993.

[24] K. Hoshino, M. Hirata, I. Kurihara, and S. Takeshima. Effects of engine oil composition on diesel particular filter. *SAE Technical Paper Series*, 2005.

[25] W. E. Audette III and V. W. Wong. A model for estimating oil vaporization from the cylinder liner ans a contributing mechanism to engine oil consumption. *SAE Technical Paper Series*, 1999.

[26] F. P. Incropera and D. P. DeWitt. *Fundamentals of Heat and Mass Transfer.* Wiley, 5th edition, 2001.

[27] J. Jocsak. The effects of surface finish of piston ring-pack performance in advanced reciprocating engines. Master's thesis, Massachusetts Institute of Technology, 2005. Available at `http://dspace.mit.edu`.

[28] T. V. Johnson. Diesel emissions control in review. *SAE Technical Paper Series*, 2008.

[29] C. Kajdas. Engine oil additives: A general overview. In W. J. Bartz, editor, *Engine Oils and Automotive Lubrication*, pages 149–176. Expert Verlag GmbH., 1993.

[30] S. R. Keleman, M. Siskin, H. S. Homan, R. J. Pugmire, and M. S. Solum. Fuel, lubricant and additive effects on combustion chamber deposits. *SAE Technical Paper Series*, 1998.

[31] J. Kim, B. Min, D. Lee, D. Oh, and J. Choi. The characteristics of carbon deposit formation in piston top ring groove of gasoline and diesel engine. *SAE Technical Paper Series*, 1998.

[32] W. Lyman, W. Reehl, and d. Rosenblatt. *Handbook of Chemical Property Estimation Methods.* American Chemical Society, 1990.

[33] M. Manni, A. Pedicillo, and F. Bazzano. A study of lubricating oil impact on diesel particular filters by means of accelerated engine tests. *SAE Technical Paper Series*, 2006.

[34] S. McGrogan. Modeling and simulation of oil transport for studying piston deposit formation in ic engines. Master's thesis, Massachusetts Institute of Technology, 2005. Available at `http://dspace.mit.edu`.

[35] Satish K. Naldu, Elmer E. Klaus, and J. Larry Duda. Kinetic model for high-temperature oxidation of lubricants. *Ind. Eng. Chem. Prod. Res. Dev.*, 24(4):596–603, 1986.

[36] K. Nishiwaki and M. Hafnan. The determination of thermal properties of engine combustion chamber deposits. *SAE Technical Paper Series*, 2000.

[37] G. Peyre. Matlab tips and tricks. 2004.

[38] M. J. Plumley. Lubricant oil consumption effects on diesel exhaust ash emissions using a sulfur dioxide treatment tracer technique and thermogravimetry. Master's thesis, Massachusetts Institute of Technology, 2005. Available at `http://dspace.mit.edu`.

[39] S. Przesmitzki. *Characterization of Oil Transport in the Power Cylinder of Internal Combustion Engines During Steady State and Transient Operation.* PhD thesis, Massachusetts Institute of Technology, 2008. Available at `http://dspace.mit.edu`.

[40] Y. Ra and R. D. Reitz. A vaporization model for discrete multi-component fuel sprays. *International Journal of Multiphase Flow*, 35:101–117, 2009.

[41] Y. Ra, R. D. Reitz, M. W. Jarrett, and T. P. Shyu. Effects of piston crevice flows and lubricant oil vaporization on diesel engine deposits. *SAE Technical Paper Series*, 2006.

[42] J. Schramm. Application of a biodegradable lubricant in diesel vehicle. *SAE Technical Paper Series*, 2003.

[43] J. Shewchuk. Delaunay refinement algorithms for triangular mesh generation. 2001.

[44] G. Strang. *Computational Science and Engineering.* Wellesley-Cambridge Press, 2007.

[45] B. Thirouard. *Characterization and Modeling of The Fundamental Aspects of Oil Transport in the Piston Ring Pack of Internal Combustion Engines.* PhD thesis, Massachusetts Institute of Technology, 2001. Available at `http://dspace.mit.edu`.

[46] H. K. Versteeg and W. Malalasekera. *An Introduction to Computational Fluid Dynamics.* Pearson Education Limited, 2nd edition, 2007.

[47] R. C. Wilhoit and B. J. Zwolinski. *Handbook of Vapor Pressures and Heats of Vaporization of Hydrocarbons and Related Compounds.* Texas A&M University, 1971.

[48] Yuichi Yamada, Masahiko Emi, Hiroyuki Ishii, Yasuko Suzuki, Shuji Kimura, and Yoshiteru Enomoto. Heat loss to the combustion chamber wall with deposit in d.i. diesel engine: variation of instantaneous heat flux on piston surface with deposit. *JSAE Review*, 23(4):415 – 421, 2002.

[49] E. Yilmaz, T. Tian, V. W. Wong, and J. B. Heywood. An experimental and theoretical study of the contribution of oil evaporation to oil consumption. *SAE Technical Paper Series*, 2002.

[50] D. Zarvalis, S. Lorentzou, and A. G. Konstandopoulos. A methodology for the fast evaluation of the effect of ash aging on diesel particulate filter performance. *SAE International*, 2009.

Appendix A

Chemical Structures of Base Stocks and Additives

All figures in Appendix A taken from [9]. Each angle shown in Figure A-1 represents a carbon atom. Some common additives shown in Figure A-2, A-3 and A-4.

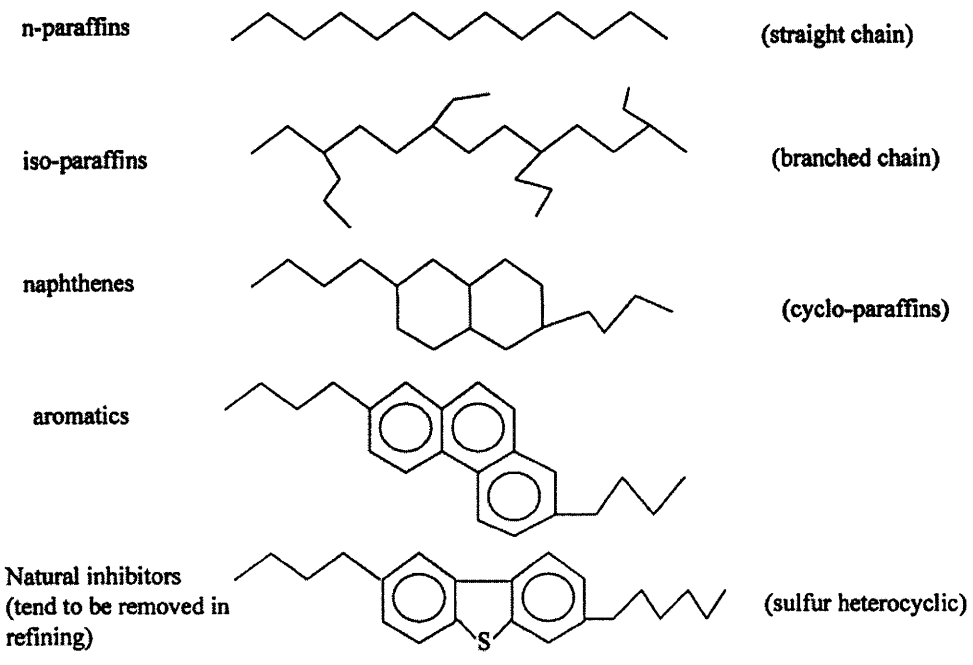

Figure A-1: Principal Hydrocarbon types in lubricants

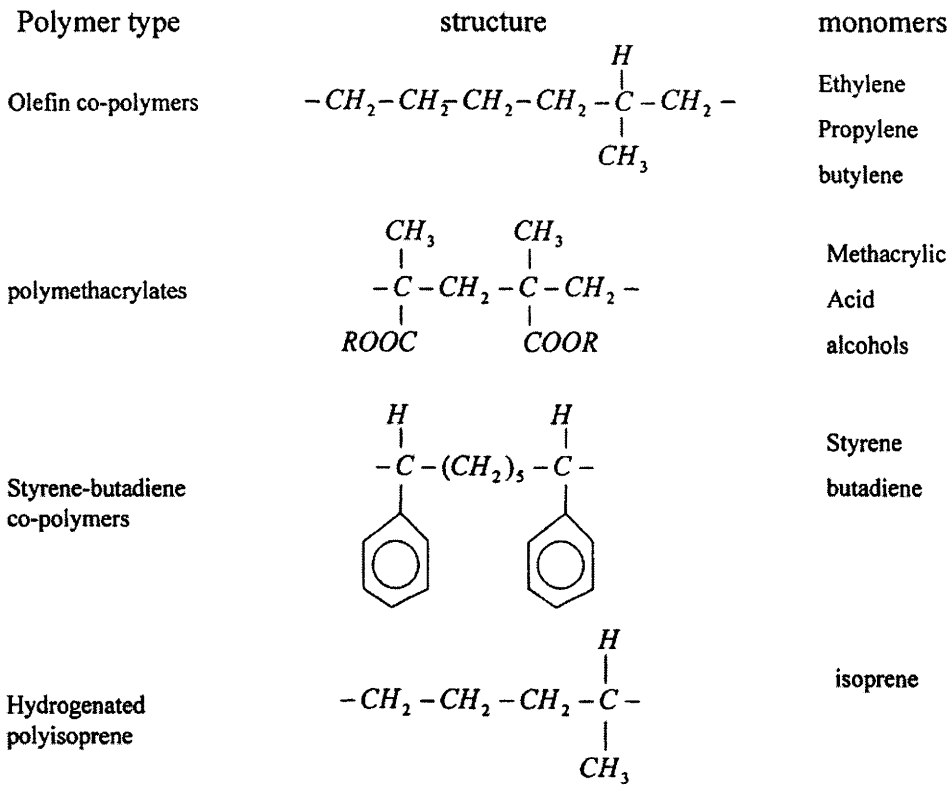

Figure A-2: Viscosity Modifiers

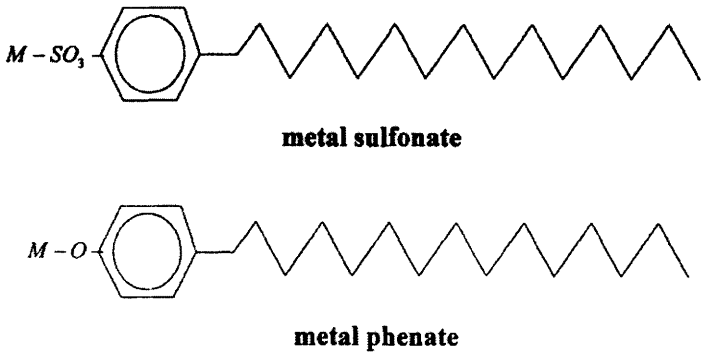

Figure A-3: Polar Detergents

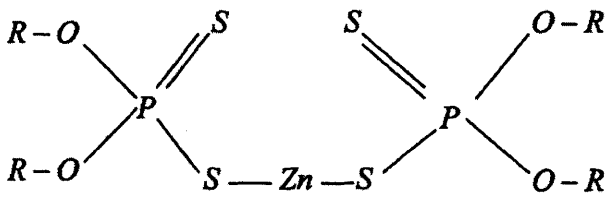

ZDDP (zinc dialkyldithiophosphates)

Figure A-4: Anti-wear ZDDP